



CrossMark
click for updates

Cite this: *RSC Adv.*, 2016, 6, 2731

Nitrogen-functionalised carbon nanotubes as a novel adsorbent for the removal of Cu(II) from aqueous solution†

Oluwaseun A. Oyetade, Vincent O. Nyamori,* Bice S. Martincigh and Sreekantha B. Jonnalagadda

This study investigated the introduction of 4'-(4-hydroxyphenyl)-2,2':6',2''-terpyridine (HO-Phttpy) onto the surface of multiwalled carbon nanotubes (MWCNTs) to obtain nitrogen-functionalized MWCNTs (MWCNT-tpty). This novel material was characterised and tested for its possible use in the remediation of wastewater contaminated with heavy metal ions. Its efficacy was compared with that of acid-functionalized MWCNTs (MWCNT-COOH) for the removal of the heavy metal ion Cu²⁺ through adsorption. HO-Phttpy was first synthesized, followed by the functionalization of MWCNT-COOH to afford MWCNT-tpty. MWCNT-tpty showed significant textural enhancement due to an increase in the extent of functionalization. This was demonstrated by an increase in the surface area and pore volume of MWCNT-tpty, from 126.8 to 189.2 m² g⁻¹ and 0.692 to 1.252 cm³ g⁻¹, respectively, relative to MWCNT-COOH. Its application for Cu²⁺ removal showed a marked increase in uptake (*q_e*), i.e. 19.44 to 31.65 mg g⁻¹, compared with MWCNT-COOH. This is attributed to the introduction of more active/chelating sites for adsorption. Adsorption experiments were conducted at pH 5 at which equilibrium was reached after 360 min. The results showed that the adsorption process was best described by the pseudo-second order model. Among the isotherms tested, the Langmuir isotherm provided the best fit for the equilibrium data. Thermodynamic studies revealed that the adsorption process was spontaneous and endothermic. Desorption studies demonstrated a better removal efficiency of Cu²⁺ from MWCNT-tpty, indicating its possible regeneration and the recovery of the Cu²⁺ adsorbate for reuse. Thus, MWCNT-tpty shows superior properties for wastewater remediation compared to MWCNT-COOH.

Received 12th November 2015
Accepted 21st December 2015

DOI: 10.1039/c5ra23900a

www.rsc.org/advances

1. Introduction

Carbon nanotubes (CNTs) are tubular shaped carbon nano-materials, possessing excellent electrical, mechanical and optical properties and thermal stability.^{1,2} They are made up of a hexagonal lattice of carbon atoms, consisting of hollow graphite, rolled at specific angles into cylinders. CNTs are classified into single-walled carbon nanotubes (SWCNTs), double-walled carbon nanotubes (DWCNTs) and multiwalled carbon nanotubes (MWCNTs), depending on the number of concentric sheets contained in the tubes.³ They form large aggregates with low dispersibility in aqueous and organic solutions due to strong van der Waals interactions between them. This requires the development of both covalent and non-covalent strategies for CNT functionalization, in order to introduce functional groups which will enhance their

application for different purposes. Covalent functionalization is often carried out through oxidation of CNTs with acids such as HNO₃ and H₂SO₄, to introduce oxygen-containing groups such as -OH and -COOH onto the walls of the tubes.⁴ This approach improves the wettability of CNTs, thereby increasing their dispersibility in aqueous/organic solutions. New functional groups, such as -NR, -F, -Cl and -SR, can also be incorporated onto the walls/sides of the tubes through solution chemistry.⁵

In recent times, the application of CNTs in various fields such as medicine, engineering, environmental science, energy, catalysis and catalyst supports, amongst many others, has been reported by various authors.^{4,6,7} This is largely attributed to their inherent properties such as large surface area, pore volume and the ease in introducing new functional groups onto their walls. In spite of these studies, functionalization of CNTs to contain multiple functional groups which will further enhance chemical reactions with other molecules is still under-researched.¹

The tridentate chelating ligand, 4'-(4-hydroxyphenyl)-2,2':6',2''-terpyridine (HO-Phttpy), containing three nitrogen atoms is a good contender for the functionalization of MWCNTs, in order to introduce nitrogen-containing donor atoms to the structure of CNTs. HO-Phttpy has profound

School of Chemistry and Physics, University of KwaZulu-Natal, Westville Campus, Private Bag X54001, Durban 4000, South Africa. E-mail: nyamori@ukzn.ac.za; Fax: +27 31 260 3091; Tel: +27 31 260 8256

† Electronic supplementary information (ESI) available. See DOI: 10.1039/c5ra23900a

flexibility to form bridged metal centres by using two or more moieties, construction of supramolecular structures and formation of macrocyclic ligands. Due to the strong affinity of this ligand for transition metal ions, the chelates produced have been used in luminescence and chemical sensing devices.⁸ In spite of the vast amount of work on CNTs, to the best of our knowledge, no study has investigated the effect of functionalization of oxidized MWCNTs (MWCNT-COOH) with HO-Phttpy for their increased activity as adsorbents.

One possible area of application of CNTs functionalized with nitrogen-donor ligands is the remediation of wastewater contaminated with heavy metal ions. In this work, the synthesized material was applied for the removal of Cu^{2+} as an example of a typical heavy metal ion discharged into the environment. The choice of copper was based on the fact that copper and its compounds are regularly used in agriculture for fertilizer production, electronics, textiles, medicine and metal cleaning purposes.⁹ The discharge of copper-contaminated effluents into aquatic environments introduces humans to necrotic changes in the liver and kidney, gastrointestinal irritations such as diarrhoea and melena, and including a number of capillary diseases; resulting in severe deleterious health effects.¹⁰ Although copper is a known essential metal at low concentrations, an excessive amount is considered harmful to both aquatic and human life.¹¹ As a result of the numerous health consequences, a variety of techniques have been used for the removal of Cu^{2+} from municipal wastewaters and industrial effluents.^{12,13} Of these methods, adsorption is considered most reliable for its removal from wastewater.¹³ This approach is simple, efficient, and cost-effective, with a high potential for recycling the metal ion and the adsorbent. Thus, the removal of Cu^{2+} from aqueous solution by adsorption has been reported through the use of tree fern,¹⁴ bagasse,¹⁵ peanut hull,¹⁶ rice husk,¹⁷ magnetite,¹⁸ peat¹⁹ and activated carbon.²⁰ Reports have shown that these adsorbents possess good potential for Cu^{2+} removal; however, drawbacks such as slow sorption and regeneration of adsorbents limits their usage.^{19,21} Pristine and functionalized CNTs have also been applied as adsorbents for Cu^{2+} removal.^{10,22,23} However, increased removal efficiency can be achieved by using CNT-based nanocomposites as adsorbents. Composites such as CNT/bagasse,²⁴ CNT/magnetite,²⁵ and CNT/chitosan²⁶ have demonstrated good sorption ability for Cu^{2+} removal. To further improve the efficiency of CNT-based nanomaterials, nitrogen-containing ligands can be used as modifiers for CNTs, hence, increasing the number of chelating sites available for adsorption on the adsorbent.¹³

In this communication, we report the synthesis of nitrogen-functionalized MWCNTs (MWCNT-ttpty) through the functionalization of acid-functionalized MWCNTs (MWCNT-COOH) by incorporating 4'-(4-hydroxyphenyl)-2,2':6',2''-terpyridine (HO-Phttpy) onto their structure. The effectiveness of this material in the adsorption of Cu^{2+} from aqueous solution was examined through a series of batch adsorption processes and compared with that of MWCNT-COOH. The effects of pH, contact time, adsorbent dose, temperature and initial Cu^{2+} concentration were investigated to determine the optimum conditions for the effective remediation of Cu^{2+} -polluted wastewater. In addition,

desorption studies were undertaken to investigate the potential reuse of the adsorbent and recovery of the adsorbate.

2. Experimental

2.1. Materials

Copper metal powder was obtained from Johnson Matthey Chemicals (Pty) Ltd (Gauteng, South Africa) while sodium hydroxide (NaOH, 98%) and sodium bicarbonate (NaHCO_3 , 99%) were purchased from Merck Chemicals (Pty) Ltd (Gauteng, South Africa). Sodium carbonate (Na_2CO_3 , 99%) was purchased from Associated Chemical Enterprises (Johannesburg, South Africa). Chemicals such as 4-hydroxybenzaldehyde (99%), 2-acetylpyridine (99%), indium bromide (InBr_3 , 99%) and solvents such as absolute ethanol, *N,N*-dimethylformamide (DMF, 99%), dimethyl sulfoxide- d_6 (DMSO- d_6 , 99%) and triethylsilane (Et_3SiH , 97%) were purchased from Sigma-Aldrich (St Louis, USA). Tetrahydrofuran (THF, 99%), chloroform (99%) and thionyl chloride (SOCl_2 , 99%) were purchased from Merck Chemicals (Pty) Ltd (Gauteng, South Africa) while aqueous ammonia (25%) was purchased from Associated Chemical Enterprises (Johannesburg, South Africa). Nitric (55%), sulfuric (98%) and hydrochloric acids (32%) were obtained from C C Imelmann Ltd (Robertsham, South Africa). All materials and chemicals were of analytical grade and used as received from suppliers without further purification. MWCNTs (purity > 95%) (P-MWCNTs), synthesized by chemical vapour deposition (CVD), were obtained from Cheap Tubes Incorporation (Brattleboro, USA).

2.2. Characterization

The ligand, 4'-(4-hydroxyphenyl)-2,2':6',2''-terpyridine, was characterized by using Fourier transform infrared (FTIR) spectroscopy, nuclear magnetic resonance (NMR) and mass spectrometry, and melting point measurements. The FTIR spectra were recorded on a Perkin Elmer RX 1 spectrophotometer and the melting point was determined by using a Bibby Stuart Scientific model SMP3 apparatus. ^1H and ^{13}C NMR spectra were obtained from a 400 MHz Bruker Avance III spectrometer and mass spectra were obtained on a Waters Synapt G2 mass spectrometer in electrospray positive mode.

Structural characterization of the adsorbents was carried out with a transmission electron microscope (TEM) (JEOL, TEM 1010) and a scanning electron microscope (SEM) (JEOL, TSM 6100) to visualize the morphology, structure, shape and size distribution of the nanomaterials. Images were captured by means of a Megaview 3 camera and analysed on iTEM software. The surface area of the adsorbents was determined with nitrogen as the flow gas by means of a Micromeritics Tristar II 3020 surface area and porosity analyser. Data were captured and analysed by using Tristar II 3020 version 2 software. Fourier transform infrared (FTIR) spectra of the synthesized materials were obtained with the samples were embedded into KBr pellets and were recorded on a Perkin Elmer Spectrum RX 1 spectrophotometer, in order to identify the surface functional groups present on the materials. Raman spectroscopy (DeltaNu

Advantage 532™) measurements were also performed to provide information on the purity and crystallinity of the adsorbents. Thermogravimetric (TGA) analyses (Q Series™ Thermal Analyzer DSC/TGA Q600) were performed to determine the thermal stability and fraction of volatile components in the samples while the Boehm titration was applied to quantitatively estimate the amount of acidic and basic groups present on the adsorbents.^{27,28} Elemental analysis (ThermoScientific Flash 2000) of adsorbents was also carried out to investigate the percentage composition of carbon, hydrogen, oxygen and nitrogen present in the samples. The point of zero charge (pH_{PZC}) was also performed as described by Oyetade *et al.*⁴ and Khan *et al.*²⁹ to estimate the electrical charge density of the adsorbents. Details of the Boehm titration and point of zero charge determination are provided in the ESI.†

2.3. Procedure for the synthesis of 4'-(4-hydroxyphenyl)-2,2':6',2''-terpyridine (HO-Phttpy)

The ligand was synthesized as reported by Patel *et al.*,^{30,31} with some modifications. 2-Acetylpyridine (2.423 g, 20.0 mmol) was added to 15 cm³ of a 2 : 1 (v/v) mixture of ethanol and water containing 4-hydroxybenzaldehyde (1.221 g, 10.0 mmol). To the solution, NaOH pellets (1.458 g, 26.0 mmol) and 30 cm³ aqueous NH₃ were added and stirred continuously at room temperature for 8 h to yield a cream-coloured precipitate. The resulting mixture was filtered, the solid obtained was washed with deionised water (5 × 10 cm³), followed by absolute ethanol (3 × 5 cm³) to obtain the crude white product (508.8 mg, 42%). m.p. 199–201 °C; IR (ATR, cm⁻¹) 3375, 1614, 1588, 1565; ¹H NMR (400 MHz, DMSO-d₆) δ : 6.92 (d, 2H, J = 8.6 Hz), 7.49–7.52 (m, 2H), 7.75 (d, 2H, J = 8.68 Hz), 7.99–8.04 (m, 2H), 8.67–8.74 (m, 6H); ¹³C NMR (400 MHz, DMSO-d₆) δ : 160.2, 155.4, 155.1, 149.4, 149.2, 137.3, 128.0, 126.8, 124.3, 120.8, 116.8, 116.4; HR-MS [C₂₁H₁₅N₃O] ES: [M + H⁺] m/z calcd 326.1215, found 326.1293. Additional spectral information is shown in ESI Fig. S1–S3.†

2.4. Preparation of MWCNT-COOH

Oxidation of MWCNTs was carried out as reported by Oyetade *et al.*⁴ and Santangelo *et al.*³² In brief, pristine MWCNTs (1.5 g) were placed in a round-bottomed flask containing 100 cm³ of concentrated hydrochloric acid, and stirred for 4 h to remove residual metal impurities from the tubes. The resulting mixture was filtered, and the solid was washed with deionised water until a neutral pH was obtained. The sample obtained was dried in a vacuum oven at 80 °C overnight and stored in a desiccator for future analysis. The purified MWCNTs were then oxidized by using a mixture of sulfuric and nitric acids in a volume ratio of 1 : 3, and refluxed at 80 °C for 12 h. The resulting mixture was diluted with deionised water, filtered, and the residue obtained was washed continuously with deionised water until a neutral pH was obtained.

2.5. Preparation of MWCNT-COCl

MWCNT-COOH (150 mg) were placed in a solution containing 30 cm³ of a 20 : 1 (v/v) mixture of SOCl₂ and dry DMF, and then

refluxed at 70 °C for 24 h. The resulting mixture was filtered and the solid washed with anhydrous THF (5 × 5 cm³).³³ The solid was dried in a vacuum oven at 80 °C, and stored under an inert atmosphere of argon for further analysis.

2.6. Preparation of MWCNT-COotpy

MWCNT-COCl (100 mg) were added to HO-Phttpy (100 mg) in a round-bottomed flask containing 20 cm³ of dry THF and 2–3 drops of glacial acetic acid. The mixture was refluxed at 64 °C for 24 h under an inert atmosphere of argon. After cooling to room temperature, the resulting suspension was filtered and the product obtained was washed with THF and dried in a vacuum oven at 80 °C overnight.

2.7. Preparation of MWCNT-ttpty

The reduction of MWCNT-COotpy to obtain an ether was carried out as reported by Sakai *et al.*³⁴ MWCNT-COotpy (100 mg), InBr₃ (10.6 mg, 0.03 mmol) and Et₃SiH (380 μ L, 2.4 mmol) were added to a 30 cm³ volume of freshly distilled chloroform, and refluxed at 60 °C for 1 h under an inert atmosphere of argon. The suspension was filtered and the solid obtained was washed with chloroform, followed by water until a neutral pH was obtained. The resulting solid was dried in a vacuum oven at 80 °C overnight and stored in a desiccator for future analysis.

2.8. Adsorbate preparation

A standard stock solution of Cu²⁺ was prepared by dissolving approximately 1.0 g of pure copper metal into 50 cm³ of 5 mol dm⁻³ nitric acid. The solution was made up to 1000 dm³ with deionised water. From this solution, working solutions were prepared by diluting the stock solution in accurate proportions to obtain the required concentrations.

2.9. Sorption experiments

The adsorption of Cu²⁺ on prepared adsorbents was investigated by using batch adsorption experiments. All adsorption experiments were conducted in duplicate by using 50 cm³ polypropylene plastic vials. Freshly prepared working solutions of 100 mg dm⁻³ Cu²⁺ were prepared from the stock solution daily. Adsorption experiments were performed by agitating 20 cm³ of a known Cu²⁺ concentration (100 mg dm⁻³) in a thermostated water bath at a fixed temperature (20 °C) for 24 h with an adsorbent dose of 50 mg. The pH of the solution was adjusted by adding appropriate amounts of 0.1 mol dm⁻³ NaOH or HNO₃ to obtain the desired pH. After the required time interval, the mixtures were filtered and the final concentration of Cu²⁺ in the filtrate was determined by inductively coupled plasma-optical emission spectroscopy (ICP-OES) (Perkin Elmer Optima 5300 DV). The effect of pH, amount of adsorbent, initial Cu²⁺ concentration, contact time and temperature was studied in order to determine the optimum conditions necessary for Cu²⁺ removal from aqueous solution. The adsorption efficiency (% adsorbed) and adsorption capacity (q_e) were calculated by using eqn (1) and (2), respectively.

$$\% \text{ adsorbed} = \left(\frac{C_i - C_{\text{eq}}}{C_i} \right) \times 100 \quad (1)$$

$$q_{\text{eq}} = \left(\frac{C_i - C_{\text{eq}}}{m} \right) \times V \quad (2)$$

C_i is the initial Cu^{2+} concentration (mg dm^{-3}), C_{eq} is the equilibrium concentration of Cu^{2+} (mg dm^{-3}), q_{eq} is the adsorption capacity (mg g^{-1}), m is the mass of the adsorbent (mg) and V is the volume (dm^3) of the adsorbate solution used.

2.9.1. Kinetics, isotherm and thermodynamic studies.

Kinetics studies were performed by agitating 20 cm^3 aliquots of $100 \text{ mg dm}^{-3} \text{ Cu}^{2+}$ solution with an adsorbent dose of 50 mg . The mixtures were placed in a thermostated water bath at $20 \text{ }^\circ\text{C}$ and agitated for different time intervals in the range of 5 to 1440 min. The pH of the solutions was adjusted to 5 by using $0.1 \text{ mol dm}^{-3} \text{ NaOH/HNO}_3$. After the pre-determined time intervals, the samples were filtered by gravity and the equilibrium concentration of Cu^{2+} determined by ICP-OES. The experimental data obtained were applied to the pseudo-first order,^{14,35} pseudo-second order,^{14,19,35,36} intraparticle diffusion³⁷ and Elovich³⁸ kinetics models. The equations for the models are given in ESI Table S1.†

Adsorption isotherms were investigated by using varying Cu^{2+} concentrations, ranging from $10\text{--}100 \text{ mg dm}^{-3}$, at a constant pH of 5. Aliquots of 20 cm^3 were mixed with 50 mg of the adsorbents and agitated on a thermostated shaking water bath under varying temperatures of 293, 303, 313 and 318 K for 24 h. The solutions were filtered by gravity and the concentrations of Cu^{2+} in the filtrates determined by ICP-OES. The experimental adsorption equilibrium data were analysed by eight adsorption isotherm models consisting of both two- (Langmuir,³⁹ Freundlich,⁴⁰ Temkin⁴¹ and Dubinin–Radushkevich⁴² models) and three-parameter (Sips,⁴³ Toth,⁴⁴ Redlich–Peterson⁴⁵ and Khan⁴⁶) models. The equations of the models are given in ESI Table S2.† Thermodynamic parameters such as change in Gibbs energy (ΔG°), change in enthalpy (ΔH°), and change in entropy (ΔS°) were also calculated over the studied temperature range.

2.9.2. Selectivity of MWCNT-tpy for different metal ions.

To investigate the selectivity of MWCNT-tpy for different metal ions, 25 cm^3 of a solution containing equal concentrations of Pb^{2+} , Zn^{2+} , Cd^{2+} and Cu^{2+} between 10 and 50 mg dm^{-3} was conditioned to pH 5.5 with the addition of appropriate amounts of $0.1 \text{ mol dm}^{-3} \text{ NaOH}$ or HNO_3 . About 200 mg of the adsorbent was added into the solution and thereafter agitated on a thermostated water bath at $20 \text{ }^\circ\text{C}$ for 24 h. The suspensions were filtered and the final concentration of metal ions in the filtrates was determined by means of ICP-OES.

2.9.3. Desorption experiments. Desorption studies were carried out by first contacting aliquots of 20 cm^3 of Cu^{2+} solution with a concentration of 100 mg dm^{-3} and an adsorbent dose of 50 mg for 24 h. The solution was filtered and the loaded-adsorbent obtained was dried in a vacuum oven at $80 \text{ }^\circ\text{C}$. The remaining Cu^{2+} concentration in the filtrate was determined. A 50 mg mass of the loaded-adsorbent was added to a 10 cm^3 aliquot of $0.1 \text{ mol dm}^{-3} \text{ HCl}$ and agitated for 30 min in

a thermostated water bath at $20 \text{ }^\circ\text{C}$. The concentration of Cu^{2+} desorbed was then determined by using ICP-OES.

2.10. Analysis of real samples

Three water samples were collected from three sites on the Umgeni river: (i) the tributary on the confluence of the Umgeni and Msunduzi rivers, (ii) the outflow from the EThekweni wastewater treatment plant and (iii) the Blue Lagoon (mouth of Umgeni rivers). The initial concentrations of Pb^{2+} , Zn^{2+} and Cu^{2+} were determined by using ICP-OES. An aliquot of 25 cm^3 of the water samples conditioned to pH 5, was measured into 50 cm^3 polypropylene bottles with an addition of 50 mg of MWCNT-tpy. The suspensions were agitated in a thermostated water bath at $20 \text{ }^\circ\text{C}$ for 1 h. After agitation, the suspensions were filtered and their supernatants analysed for the final concentrations of metal ions in solution. The removal efficiency and adsorption capacity for each metal ion were evaluated according to eqn (1) and (2), respectively.

2.11. Data analysis

The data obtained were fitted to the isotherm and kinetics models by means of the nls nonlinear regression routine in the R statistical computing environment.⁴⁷ The R statistical software takes into account the minimization of the sum of squared residuals (SSR) and the residual square errors (RSE). A comparison of all SSR and RSE values was done in order to assess the adequacy of the models. The model chosen was that with the lowest SSR.

3. Results and discussion

The ligand and nanomaterials synthesised were characterized by a series of techniques to ascertain the authenticity and properties of the adsorbents for Cu^{2+} removal. Subsequently, the efficiency of the novel material to adsorb Cu^{2+} was assessed and compared with that of acid-functionalized MWCNTs by means of batch adsorption processes.

3.1. Synthesis of 4'-(4-hydroxyphenyl)-2,2':6',2''-terpyridine (HO-Phttpy)

The synthesis of 4'-(4-hydroxyphenyl)-2,2':6',2''-terpyridine was carried out by using a “greener” synthetic approach as illustrated in Fig. 1. The use of green solvents such as ethanol and water at room temperature affords an opportunity of obtaining products in moderate yields. Upon reacting 4-hydroxybenzaldehyde and 2-acetylpyridine in an ethanolic solution, a cream-coloured precipitate was formed. The completion of the reaction was monitored by thin layer chromatography (TLC) and FTIR and NMR spectroscopy. The formation of the product was confirmed by the disappearance of the carbonyl absorption band at $\approx 1700 \text{ cm}^{-1}$ and the appearance of sharp peaks at 1634 cm^{-1} (C=N str), $1250\text{--}1335 \text{ cm}^{-1}$ (C–N str), 712 cm^{-1} and 634 cm^{-1} (indicating γ and δ Py-ring in-plane and out-of-plane deformation vibrations respectively) in the FTIR spectra (Fig. 4c).^{48–50} ^1H NMR spectrometry further confirmed the formation of the product by the disappearance of the methyl

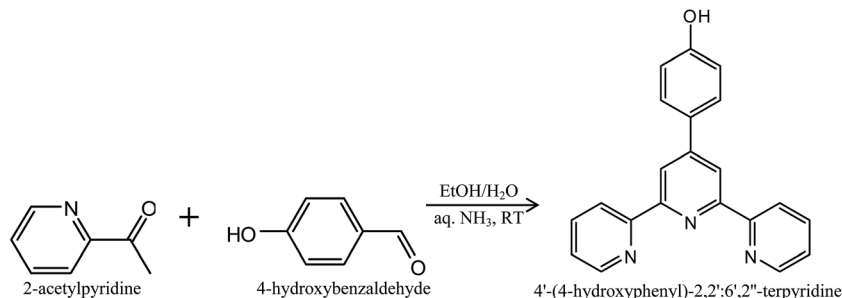


Fig. 1 Synthesis of 4'-(4-hydroxyphenyl)-2,2':6',2''-terpyridine (HO-Phttpy).

proton resonance peak (≈ 2.10 ppm) and the appearance of aromatic proton resonance peaks (≈ 7.5 – 8.0 ppm) (see ESI Fig. S1†). Further verification of the product was done by ^{13}C NMR and mass spectroscopy (see ESI Fig. S2 and S3†).

3.2. Synthesis of MWCNT-ttpty

The synthesis of the novel nanomaterial was carried out first by the acylation of MWCNT-COOH with a mixture of SOCl_2 and DMF in a volume ratio of 20 : 1 as illustrated in Fig. 2.

Acylation of nanotubes (MWCNT-COCl) were further reacted in a mass ratio of 1 : 1 with HO-Phttpy to afford esterified MWCNTs (MWCNT-COOptpy). Reduction of MWCNT-COOptpy was carried out in distilled CHCl_3 , by using Et_3SiH as a reducing agent and InBr_3 as a catalyst, to afford ether-functionalized CNTs (MWCNT-ttpty). The route to the synthesis of MWCNT-ttpty is shown in Fig. 3.

3.3. Characterization of adsorbents

The synthesized products were characterized by FTIR spectroscopy. Fig. 4 shows the FTIR spectra of (a) P-MWCNT, (b) MWCNT-COOH, (c) HO-Phttpy and (d) MWCNT-ttpty. For pristine MWCNTs (P-MWCNTs), the peaks observed at $\approx 1498\text{ cm}^{-1}$ are assigned to $\text{C}=\text{C}$ stretching vibrations (Fig. 4a) which are representative of graphitic structures characteristic of CNTs.¹ The peaks observed around ≈ 3500 and $\approx 2700\text{ cm}^{-1}$ are attributed to the presence of water molecules and carbon dioxide, respectively. Acidic functional groups such as carboxylic groups were introduced onto the walls of tubes after oxidation, hence a new peak at $\approx 1750\text{ cm}^{-1}$, assigned to $\text{C}=\text{O}$ stretching, was noticeable (Fig. 4b), indicating the presence of new groups after oxidation was carried out.²³ For HO-Phttpy (Fig. 4c), peaks at 3050 cm^{-1} (aromatic $\text{C}-\text{H}$ str), 1475 – 1585 cm^{-1} (aromatic $\text{C}=\text{C}$ str), 1634 cm^{-1} ($\text{C}=\text{N}$ str), 2890 –

2970 cm^{-1} (CH_2 and CH groups), 3500 cm^{-1} ($\text{O}-\text{H}$ str), 1250 – 1335 cm^{-1} ($\text{C}-\text{N}$ str), 712 cm^{-1} and 634 cm^{-1} (indicating γ and δ Py-ring in-plane and out-of-plane deformation vibrations respectively) were obtained.^{48–50} Of importance to note is that MWCNT-ttpty (Fig. 4d) showed a similar profile to that of the ligand (Fig. 4c). This therefore confirms that the successful functionalization of MWCNT-COOH with HO-Phttpy was achieved, since functional groups characteristic to the ligand were present for MWCNT-ttpty.

To confirm the shape and structure, and determine the morphology of the synthesized adsorbents, images were collected from transmission electron microscopy (TEM) and scanning electron microscopy (SEM). The micrographs shown in Fig. 5 represent the SEM images of (a) P-MWCNT, (b) MWCNT-COOH and (c) MWCNT-ttpty while Fig. 6 shows the TEM images of (a) P-MWCNT, (b) MWCNT-COOH and (c) MWCNT-ttpty. As shown in Fig. 5a and 6a, a large entanglement of tubes was observed for P-MWCNT demonstrating a high presence of metal catalyst (shown with arrows) and amorphous carbon on the surface of the tubes. More alignment and less agglomeration was observed for MWCNT-COOH (*i.e.* tubes purified and functionalized with acids) (Fig. 5b). This is in agreement with the study of Rosca *et al.*⁵¹ Oxidation of CNTs accounts for the shortening of tubes, thereby introducing new functional groups, such as carboxylate groups, onto open ends of CNTs. Purification of CNTs removes the metal catalyst and amorphous carbon present on the surface of the tubes.¹ Also, Fig. 6c further demonstrates that the tubular structure characteristic of MWCNTs was preserved after functionalization with the nitrogen ligand was carried out. A higher interspaced region was also noticed between tubes when compared with MWCNT-COOH (Fig. 5b vs. c). The images shown in Fig. 6a and b demonstrate the straight morphology for P-MWCNTs and MWCNT-COOH, while a curved/bent morphology was obtained

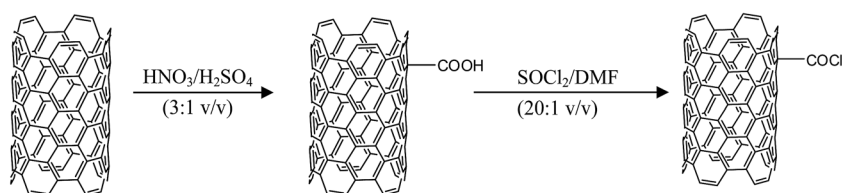


Fig. 2 Acylation of pristine MWCNTs.

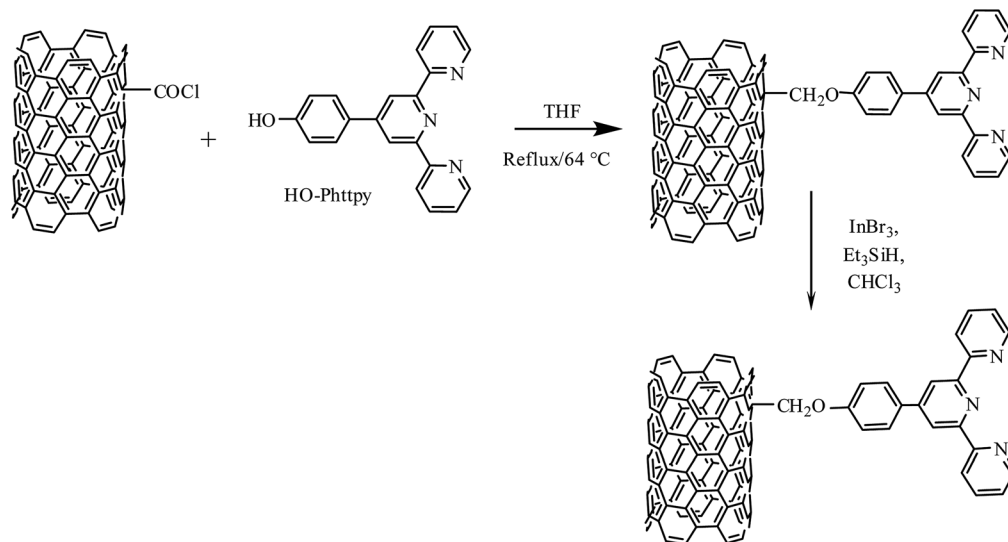


Fig. 3 Route to the synthesis of MWCNT-ttpy.

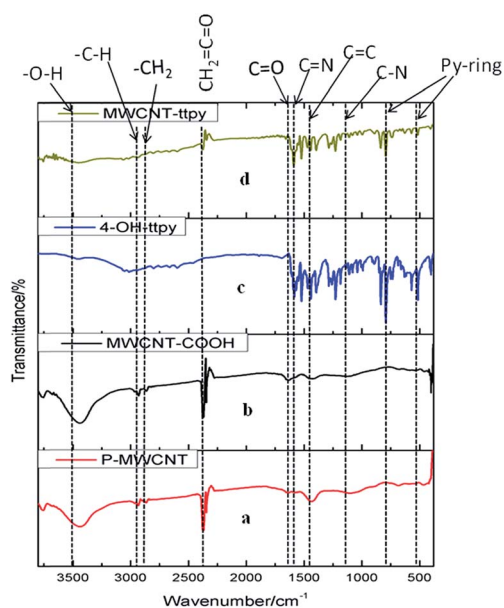


Fig. 4 FTIR spectra of (a) P-MWCNT, (b) MWCNT-COOH, (c) HO-Phttpy and (d) MWCNT-ttpy.

for MWCNT-ttpy (Fig. 6c) due to the introduction of the ligand. Evidence of functionalization was also noted as long strands of CNTs were cut to obtain short and open-ended tubes.

In order to establish the thermal stability, purity and amount of volatile components in the synthesized adsorbents, thermogravimetric analysis (TGA) was carried out. Fig. S4[†] represents the (a) thermograms (TGA) and (b) derivative thermograms (DTG) of P-MWCNT, MWCNT-COOH and MWCNT-ttpy. As observed from Fig. S4a,[†] both P-MWCNTs and MWCNT-COOH were more thermally stable than MWCNT-ttpy. A lower decomposition temperature was obtained for MWCNT-ttpy than for P-MWCNTs and MWCNT-COOH (Fig. S4a[†]). This could be attributed to the increase in defects induced by the functionalization of MWCNT-COOH. This result is consistent with data obtained from Raman spectroscopy (Table 1), which demonstrates that MWCNT-ttpy had a higher I_D/I_G ratio than either P-MWCNTs or MWCNT-COOH. A higher ratio was also obtained for MWCNT-COOH when compared with P-MWCNTs. Hence, decreasing crystallinity in MWCNT-COOH and MWCNT-ttpy was associated with increasing functionalization, which thereby induces an increase in defects on P-MWCNTs, resulting in a larger I_D/I_G ratio. An increase in defective sites also accounts for a decrease in the decomposition temperature of

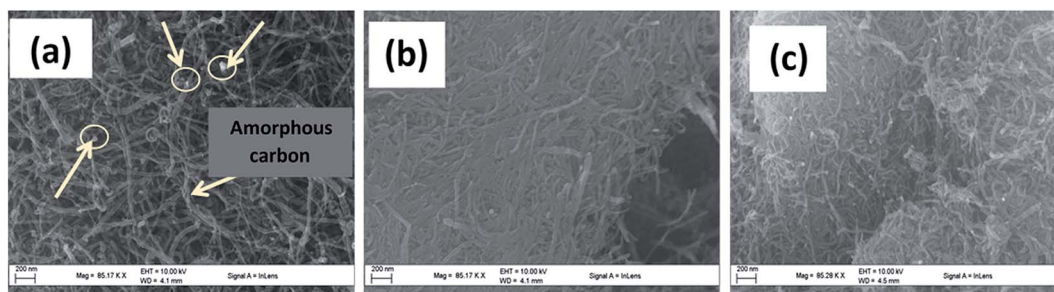


Fig. 5 SEM images of (a) P-MWCNT, (b) MWCNT-COOH and (c) MWCNT-ttpy.

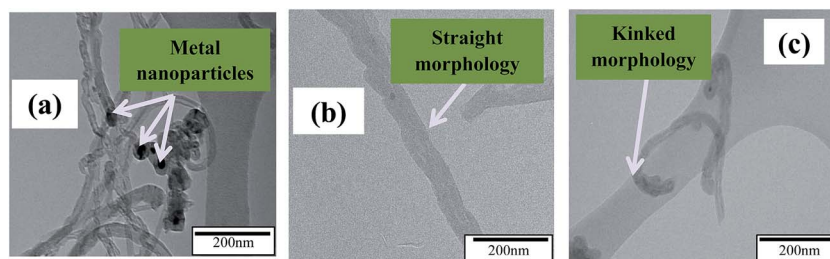


Fig. 6 TEM images of (a) P-MWCNT, (b) MWCNT-COOH and (c) MWCNT-ttpty.

MWCNT-COOH and MWCNT-ttpty obtained from TGA. The thermal stability of MWCNTs therefore increased in the order MWCNT-ttpty < MWCNT-COOH < P-MWCNTs. These results are consistent with recently published studies by Zhao *et al.*,¹ Ombaka *et al.*,⁷ and Chizari *et al.*,⁵² indicating that increasing functionalization results in a reduced decomposition temperature and larger I_D/I_G ratio. Purification of P-MWCNTs also resulted in the decrease of metal catalyst present in MWCNT-COOH (Fig. S4a†) as indicated by the residual mass remaining after 620 °C. Three thermal decomposition stages were obtained for MWCNT-ttpty. The first stage (in circle) showed a mass loss ($\Delta m = 9.88\%$) in the interval of 282–412 °C, suggesting the release of CH_4O (9.85%, calcd). The second decomposition step (shown with arrow) demonstrates a mass loss ($\Delta m = 35.84\%$) in the temperature range of 434–555 °C, suggesting the release of C_9H_6 (35.08%, calcd). The third decomposition step was observed for all three types of CNTs (*i.e.* P-MWCNTs, MWCNT-COOH and MWCNT-ttpty), representing the total decomposition of the graphitic structure of CNTs.

The surface area of the adsorbents was noticed to increase in the order P-MWCNTs < MWCNT-COOH < MWCNT-ttpty (Table 1). The results obtained indicated an increase in surface area and pore volume of MWCNT-COOH when compared with P-MWCNT (Table 1, Entry 2 *vs.* 1). This is attributed to the treatment of P-MWCNT, which results in cutting of large entanglements of tubes (Fig. 6a), thereby causing an increase in surface area and pore volume as observed in MWCNT-COOH.⁷ Furthermore, an increase in surface area and pore volume of MWCNT-ttpty (Table 1, Entry 3 *vs.* 2) was obtained, due to increasing functionalization of MWCNT-COOH. This result confirms that surface area/pore volume of nanomaterials can be increased based on the extent of functionalization. All adsorbents were mesoporous in nature since the pore diameters were less than 50 nm. Hence, MWCNT-COOH and MWCNT-ttpty possess moderately large surface areas and increased pore volume, which might enhance faster and better sorption ability

of the adsorbents for the removal of Cu^{2+} from aqueous solutions.

Elemental analysis of the adsorbents confirmed the presence of nitrogen atoms attached to the ligand on the MWCNT-ttpty. However, as expected, nitrogen atoms were absent in P-MWCNTs and MWCNT-COOH (Table S3†). Thus, the presence of nitrogen atoms in MWCNT-ttpty confirms the successful functionalization of MWCNT-COOH with HO-Phttpty. The elemental analysis also showed an increase in the amount of oxygen in the order P-MWCNTs < MWCNT-COOH < MWCNT-ttpty. Acidic functionalization of P-MWCNTs accounts for the increase in the oxygen content of MWCNT-COOH due to the incorporation of oxygen-containing functional groups onto the walls of tubes.⁴ An increase in the oxygen content of MWCNT-ttpty is accounted for by the functionalization of MWCNT-COOH, which introduces nitrogen and more oxygen atoms onto the tubes. This result is consistent with data obtained from the Boehm titration (Table 2) which demonstrates an increase in the surface acidic groups of the MWCNTs as the extent of functionalization increases.

The nature of the acidic and basic functional groups on the adsorbents was determined by the Boehm titration method.^{28,53} Functionalization of P-MWCNT with acids markedly increased the concentration of carboxyl, phenolic and lactonic groups on MWCNT-COOH (Table 2). This was consistent with the FTIR spectra (Fig. 4b) obtained, which revealed the appearance of a new peak at $\approx 1750\text{ cm}^{-1}$ corresponding to the formation of carboxylic groups. This result conforms with data reported by Biniak *et al.*²⁷ wherein an increase in acidic properties was attributed to oxidation of adsorbents with acids. However, further functionalization with the nitrogen ligand decreased the concentration of the carboxyl groups but increased the concentrations of phenolic and lactonic groups. It is also worthy of note that an increase in the total number of basic groups of the adsorbents was observed as the extent of functionalization increased. MWCNT-ttpty contained the largest amount of basic

Table 1 Textural characterization of synthesized nanomaterials

Entry	Adsorbents	Surface area/ $\text{m}^2\text{ g}^{-1}$	Pore volume/ $\text{cm}^3\text{ g}^{-1}$	Pore diameter/nm	I_D/I_G
1	P-MWCNT	108.8	0.494	18.44	1.17
2	MWCNT-COOH	126.8	0.692	22.95	1.19
3	MWCNT-ttpty	189.2	1.252	27.26	1.31

Table 2 Surface chemistry of P-MWCNTs, MWCNT-COOH and MWCNT-ttpty determined by the Boehm titration method

Adsorbents	Carboxyl/ mmol g ⁻¹	Lactonic/ mmol g ⁻¹	Phenolic/ mmol g ⁻¹	Total acidic groups/ mmol g ⁻¹	Total basic groups/ mmol g ⁻¹	pH _{PZC}
P-MWCNTs	0.136	0.014	0.114	0.264	0.145	5.04
MWCNT-COOH	0.719	0.104	0.401	1.224	0.226	4.02
MWCNT-ttpty	0.613	0.165	0.544	1.322	0.752	4.48

groups justifying the presence of nitrogen-containing groups on the adsorbent.

3.4. Batch adsorption processes

Sorption processes were carried out to examine the effectiveness and efficiency of MWCNT-COOH and MWCNT-ttpty for the removal of Cu²⁺ from a simulated wastewater. The role of various parameters that influence adsorption such as pH, contact time, adsorbent dose, temperature and initial adsorbate concentration were investigated to ascertain the ideal conditions suited for Cu²⁺ removal. Kinetics, isotherm and thermodynamic studies were also carried out by using the data obtained.

3.4.1. Effect of pH. The extent of adsorption of Cu²⁺ onto the studied adsorbents was investigated at different pH values ranging from 1.0 to 10.0. Removal of Cu²⁺ from aqueous solution is usually influenced by the initial pH of the solution, since it influences the surface charges present on the adsorbent and the speciation of the metal ion in solution.⁵⁴ Fig. 7b shows the speciation of Cu²⁺ as a function of pH in aqueous solution. Free Cu²⁺ exist only at pH values ≤ 5. Precipitation of Cu²⁺ as hydroxy species occurs when the pH of the solution is further increased.

A significant increase is noticed for the removal of Cu²⁺ from aqueous solution as the pH of the solution is increased (Fig. 7a). The surface charge of the adsorbents is positive at pH values less than their pH_{PZC} (Table 2), resulting in a low removal of the adsorbate due to strong competitive activity between Cu²⁺ and

H⁺ ions for active sites on the adsorbent. Increasing the pH of the solution led to a decrease in H⁺, which enabled electrostatic/coordination attraction of Cu²⁺ onto the active sites of the adsorbents. Cationic adsorption is favourable at pH values higher than pH_{PZC};⁵⁵ hence, sorption of Cu²⁺ was propitious at pH conditions greater than 4.5. Higher removal efficiencies of Cu²⁺ were noticeable from pH 3 to 7 when MWCNT-ttpty was used as adsorbent. This is attributed to an increase in the number of chelating sites on the adsorbent, which permits strong binding between the nitrogen-donor atoms in the adsorbent and Cu²⁺. Modification of MWCNT-COOH with HO-Phttpty significantly improved the textural properties of MWCNT-COOH, resulting in an increase in surface area, pore volume (Table 1) and active sites on MWCNT-ttpty (Table 2), hence, enabling better sorption ability for Cu²⁺ removal. Although the data suggest that pH 7 is optimal for the removal of Cu²⁺, further adsorption studies were carried out at a pH value of 5, in order to limit the effect of precipitation on Cu²⁺ removal.

3.4.2. Effect of contact time. The effect of contact time for the adsorption of Cu²⁺ was examined at varying time intervals, between 5 and 1440 min, while keeping the initial Cu²⁺ concentration (100 mg dm⁻³), pH (5.0) and adsorbent dose (50 mg) constant. The percentage removal of Cu²⁺ onto the studied adsorbents was noticeably increased with time, attaining equilibrium for MWCNT-COOH and MWCNT-ttpty at 180 min and 360 min, respectively (Fig. 8). After this stage, the percent adsorption was observed to remain steady with little or no further increase. Initially, more active sites are available for adsorption, hence, enabling faster removal. As the binding sites

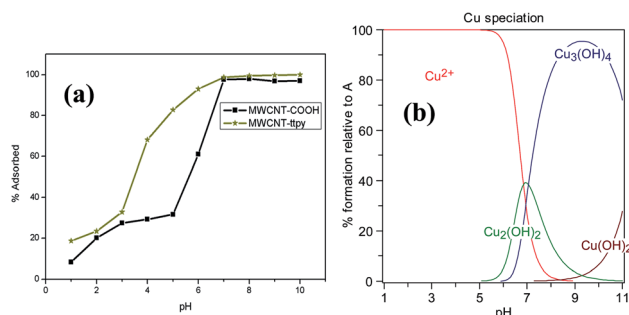


Fig. 7 (a) Effect of pH on sorption of Cu²⁺ onto MWCNT-COOH and MWCNT-ttpty, [conditions: 20 cm³ of 100 mg dm⁻³ Cu²⁺, 24 h equilibration time, 50 mg adsorbent dose, agitation speed 150 rpm, temperature 20 °C] and (b) speciation of Cu²⁺ as a function of pH in aqueous solution. Numerical values of log β for the metal hydroxides used in the calculation of the speciation curves were obtained from critical stability constants compiled by Smith and Martell,⁵⁶ and plots obtained with the aid of HySS software.⁵⁷

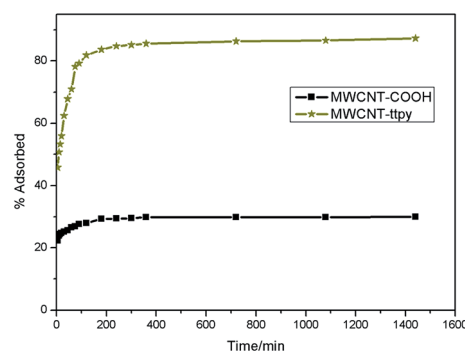


Fig. 8 Effect of contact time for the adsorption of Cu²⁺ onto MWCNT-COOH and MWCNT-ttpty [conditions: 20 cm³ of 100 mg dm⁻³ Cu²⁺, 50 mg adsorbent dose, pH 5.0, agitation speed 150 rpm, temperature 20 °C].

on the surface of the adsorbents were occupied, further removal of Cu^{2+} was observed to be minimal. Though adsorption was rapid in both adsorbents, MWCNT-ttpy exhibited higher removal efficiency at each time than MWCNT-COOH. This could be attributed to the greater number of chelating sites on MWCNT-ttpy, induced through the functionalization of MWCNT-COOH with a nitrogen-containing compound. In this study, the maximum time for agitation was fixed at 24 h to ascertain the complete removal of Cu^{2+} from aqueous solutions under all conditions.

3.4.3. Kinetics studies. Four kinetics models, namely, the pseudo-first order, pseudo-second order, Elovich and intraparticle diffusion models were applied to the experimental data in order to determine the dynamics and rate-determining step of the adsorption process. Table S1† gives the equations of the models used in this study. The experimental data obtained were fitted into the kinetics models by non-linear least squares (NLLS) analysis. Previous studies have shown that to eliminate error distributions associated with models in linearized forms, NLLS analysis^{58–60} is a preferred choice. The curves showing a comparison of all the kinetics models fitted for the adsorption of Cu^{2+} onto MWCNT-COOH and MWCNT-ttpy are shown in ESI Fig. S5.† Data illustrating the comparison of all models with their associated sum of squared residuals (SSR) and residual square errors (RSE) is given in Table 3. It was observed that the data for MWCNT-ttpy best fit the pseudo-second order model, while that for MWCNT-COOH fit the Elovich model better as reflected by the lowest SSR values (Table 3). The pseudo-second order model assumes that the rate-limiting step for Cu^{2+} adsorption may be due to interaction through sharing or exchange of electrons between hydroxyl/nitrogen groups and Cu^{2+} .^{14,26,36,61} Hence, this indicates that the rate of removal of Cu^{2+} from aqueous solution was determined by a bimolecular interaction between the adsorbate and active sites on the

adsorbents. Similar results have been reported by Ho and McKay,⁶¹ Popuri *et al.*²⁶ Mobasherpour *et al.*¹⁰ and Yu *et al.*⁶² for removal of Cu^{2+} from aqueous solutions. The Elovich model is also based on the concept of chemisorption³⁶ (*i.e.* the interaction through sharing or exchange of electrons). This further elucidates that the adsorption of Cu^{2+} onto both adsorbents proceeds *via* chemical interactions between the active groups on the adsorbents and cationic Cu^{2+} .

Adsorption proceeds *via* one/more of these four stages: (i) the transfer of solute from the solution to the surface of the adsorbent, (ii) solute transfer from the bulk solution to the boundary film which surrounds the adsorbent surface (film diffusion), (iii) solute transfer through the internal pores of the adsorbent (intraparticle diffusion), and (iv) interaction between adsorbate molecules with the active sites on the external surface of the adsorbent. One of these processes usually determines the rate at which the adsorbate is removed from aqueous solutions. To further elucidate the diffusion mechanism involved in adsorption, experimental data were modelled with the intraparticle diffusion model. A plot of q_t against \sqrt{t} plotted to obtain a straight line which did not pass through the origin. This indicates that adsorption proceeded through the intraparticle diffusion of Cu^{2+} to the pores of the adsorbent; however, it was not the only rate-controlling step.^{63–65} Adsorption therefore occurred *via* a multi-step process involving an initial rapid stage, followed by the intraparticle diffusion of adsorbates to the pores of adsorbents and then to a slower phase which proceeds towards saturation due to low adsorbate concentration.⁵⁸ Higher k_{id} and l values were obtained for MWCNT-ttpy than MWCNT-COOH, showing that adsorption was boundary-controlled and indicates better Cu^{2+} removal for MWCNT-ttpy.

3.4.4. Effect of adsorbent dose. The effect of increasing the amount of adsorbent on Cu^{2+} ion removal was investigated at varying adsorbent dosage ranging from 30–400 mg. An increase in the percentage removal of Cu^{2+} was achieved as the mass of adsorbent increased, until a limiting value was reached, where removal remained steady (Fig. 9). This is attributed to the fact that as the dose of adsorbent increases, there is an increase in the surface area and number of active sites available for adsorption. A high efficiency of Cu^{2+} removal was obtained for MWCNT-ttpy with percentages in the range of 80 to 100% being obtained in contrast to 60% for MWCNT-COOH. This illustrates that complete removal of Cu^{2+} can be achieved with MWCNT-ttpy; hence, it has promising applications for remediating wastewater generated from industries. The increase in the number of metal binding sites on MWCNT-ttpy is responsible for the high removal of Cu^{2+} observed. An adsorbent dose of 100 mg of MWCNT-ttpy achieved 99% removal efficiency, after which a state of equilibrium was reached with increase in adsorbent dose due to the limited amount of Cu^{2+} in solution. This state of equilibrium was achieved with a dose of 300 mg for MWCNT-COOH. However, it is worthy of note that as the dose of adsorbent is increased, the adsorption capacity (q_{eq}) decreased for both adsorbents. This is due to the fact that increasing the adsorbent dose at the same concentration and volume of adsorbate solution leads to unsaturation of adsorption sites.

Table 3 Kinetics parameters for the adsorption of divalent copper ion from aqueous solution

Model	Parameter	MWCNT-COOH	MWCNT-ttpy
Pseudo-first order	k_1/min^{-1}	0.259	0.073
	$q_{eq}/\text{mg g}^{-1}$	10.06	33.30
	RSE ^a	0.741	3.350
	SSR ^b	8.242	168.3
Pseudo-second order	$k_2/\text{g mg}^{-1} \text{min}^{-1}$	0.044	0.003
	$q_{eq}/\text{mg g}^{-1}$	10.44	35.25
	RSE	0.447	1.858
	SSR	2.994	51.77
Intraparticle diffusion	$k_{id}/\text{mg g}^{-1} \text{min}^{-0.5}$	0.491	1.573
	$l/\text{mg g}^{-1}$	7.764	14.66
	RSE	5.639	15.64
	SSR	508.8	3916
Elovich	$\alpha/\text{mg g}^{-1} \text{min}^{-1}$	5.237	192.7
	$\beta/\text{g mg}^{-1}$	1.864	0.287
	RSE	0.217	2.082
	SSR	0.705	65.00

^a RSE – residual square error. ^b SSR – sum of squared residuals.

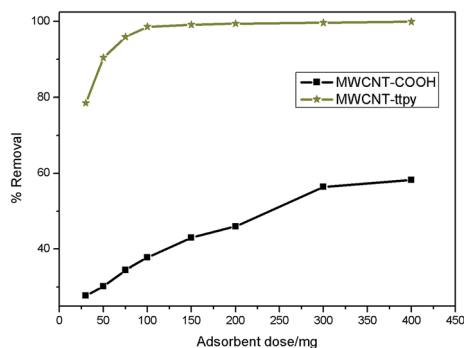


Fig. 9 Effect of adsorbent dose for the adsorption of Cu^{2+} onto MWCNT-COOH and MWCNT-tpy [conditions: 20 cm^3 of $100 \text{ mg dm}^{-3} \text{ Cu}^{2+}$, 24 h equilibration time, pH 5.0, agitation speed 150 rpm, temperature $20 \text{ }^\circ\text{C}$].

3.4.5. Effect of initial adsorbate concentration. The influence of increasing the adsorbate concentration was examined for different Cu^{2+} concentrations, ranging from $10\text{--}100 \text{ mg dm}^{-3}$, on MWCNT-COOH and MWCNT-tpy. A decrease in the percentage removal of Cu^{2+} from 98.2% to 47.6% and 100.0% to 78.9% was obtained for MWCNT-COOH and MWCNT-tpy, respectively. This could be attributed to the greater number of active sites available at lower Cu^{2+} concentrations, resulting in higher removal efficiencies. However, saturation of active sites occurred at higher concentrations, resulting in lower removal efficiencies. Also, an increase in the amount of Cu^{2+} removed per unit mass from 3.87 to 19.01 mg g^{-1} and 3.94 to 31.89 mg g^{-1} was obtained for MWCNT-COOH and MWCNT-tpy, respectively. Higher initial concentrations of Cu^{2+} enhanced the adsorption process, due to an increase in the driving force by overcoming mass transfer resistance between the solid–solution interface.⁵⁴ Similar trends for the removal of Cu^{2+} from aqueous solution as concentration is varied have been reported by Tong *et al.*⁵⁴ Ekmekyapar *et al.*⁶⁶ and Yu *et al.*⁶²

3.4.6. Effect of temperature. Increasing the adsorbate temperature results in an increase in the rate of diffusion across the external boundary layer, decreases the viscosity of the solution and increases the internal pores of the adsorbents.⁶⁷ The extent of adsorption was investigated over the temperature range of $293\text{--}318 \text{ K}$. An increase in the adsorption capacity (q_{eq}) with an increase in temperature was obtained for MWCNT-tpy (Fig. 10b), whereas a decrease in q_{eq} was obtained with increasing temperature for MWCNT-COOH (Fig. 10a). An increase in temperature favours faster mobility of Cu^{2+} , as was the case for MWCNT-tpy, hence resulting in higher q_{eq} values. Also, higher Cu^{2+} uptake by MWCNT-tpy at higher temperatures may be attributed to an increase in the porosity and pore volumes of the adsorbent, hence, enabling the pores for better uptake of adsorbate.⁴ However, increasing the adsorbate temperature also results in a decrease of the physical adsorptive forces responsible for adsorption. This phenomenon was observed for MWCNT-COOH (Fig. 10a), and resulted in a decrease in q_{eq} values as the temperature of the adsorbate increased. Fig. 10a also showed a significant change in q_{eq} with

temperature variation for MWCNT-COOH, whereas very little effect was observed for MWCNT-tpy with change in temperature (Fig. 10b). This illustrates that MWCNT-tpy will be effective for Cu^{2+} removal, and could prove advantageous regardless of change in temperature. Also, the application of MWCNT-tpy will be sufficient for the removal of Cu^{2+} at point source, as effluents are normally discharged at above ambient temperatures. It is also worthy of note that the amount adsorbed (q_{eq}) by MWCNT-tpy was also greater than for MWCNT-COOH at all temperatures.

3.4.7. Adsorption isotherms. Adsorption isotherms are usually used to describe how adsorbate molecules/ions interact with the active sites on the surface of the adsorbent and to optimize adsorbent use for large-scale removal.⁴ Eight isotherms, including two- and three-parameter models, namely, Langmuir, Freundlich, Temkin, Dubinin–Radushevick (D–R), Sips, Toth, Redlich–Peterson (R–P) and Khan, were applied to the equilibrium data obtained in this study. The equations for the isotherms are given in Table S2.† NLLS analysis was used to fit the data and the lowest sum of squared residuals (SSR) gave an indication of the best fit for the equilibrium data obtained. The parameters obtained for the adsorption of Cu^{2+} onto MWCNT-COOH and MWCNT-tpy are presented in Table 4.

Table 4 demonstrates that the Freundlich isotherm best describes the experimental data obtained for MWCNT-COOH, while the Langmuir isotherm best described the data obtained for MWCNT-tpy. The curves for the best-fit isotherms for MWCNT-COOH and MWCNT-tpy are shown in ESI Fig. S6 and S7,† respectively. The Langmuir maximum adsorption capacity (q_{m}) varied from 15.50 to 19.44 mg g^{-1} and 31.65 to 34.13 mg g^{-1} for MWCNT-COOH and MWCNT-tpy, respectively over the studied temperature range. Table 4 further indicates a decrease in q_{m} as the temperature of the adsorbate solution was increased for MWCNT-COOH, whereas an increase in q_{m} was obtained with increasing temperature for MWCNT-tpy. The Langmuir adsorption constant, b (Table 4), indicating the high adsorptive binding power obtained for MWCNT-tpy, is indicative of good adsorptive forces resulting in the enhancement of the binding strength as the temperature is increased.

The amount of area on the adsorbent covered by Cu^{2+} can be established by dividing the theoretical specific surface area (S) into the BET surface area. The theoretical surface area was calculated by using eqn (3) as described by Ho *et al.*⁶⁸

$$S = \frac{q_{\text{m}} N_{\text{A}} A}{M} \quad (3)$$

S is the area covered by the adsorbed Cu^{2+} , N_{A} is Avogadro's constant, A is the cross-sectional area of Cu^{2+} ($1.58 \times 10^{-20} \text{ m}^2$)⁶⁸ and M is the molar mass of Cu^{2+} . The values obtained for S at $20 \text{ }^\circ\text{C}$ for MWCNT-COOH and MWCNT-tpy were calculated as 2.91 and $4.74 \text{ m}^2 \text{ g}^{-1}$, respectively. As given by Table 1, the BET surface area of MWCNT-COOH and MWCNT-tpy was 126.8 and $189.2 \text{ m}^2 \text{ g}^{-1}$, respectively. Hence, the percentage of adsorbent surface covered by Cu^{2+} was calculated as 2.30% and 2.51% , respectively. Equally, q_{m} values at $20 \text{ }^\circ\text{C}$ were compared with the total number of acidic and basic groups in MWCNT-COOH and MWCNT-tpy determined by the Boehm titration

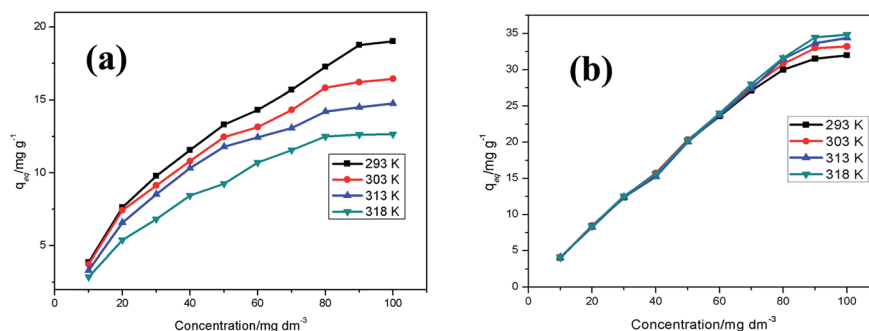


Fig. 10 Effect of varying temperature on the adsorption of Cu^{2+} by (a) MWCNT-COOH and (b) MWCNT-ttpy.

(Table 2). The values obtained indicated that 25.0% of acidic groups on MWCNT-COOH and 66.2% of basic groups on MWCNT-ttpy were primarily involved in adsorption of Cu^{2+} onto active sites of adsorbents. These results indicate that chelation of Cu^{2+} with nitrogen-donor atoms in MWCNT-ttpy and electrostatic interactions with oxygen atoms in MWCNT-COOH were primarily responsible for interaction in this study. Hence, adsorption of Cu^{2+} could be said to be enhanced significantly due to the presence of N donor atoms on MWCNT-ttpy.

Also, as suggested by Hamza *et al.*⁶⁹ and Soon-An *et al.*,⁷⁰ the nature of the adsorption process can be estimated depending on the values of the separation factor (R_L) as expressed in eqn (4). Adsorption is assumed to be favourable if $0 < R_L < 1$, unfavourable if $R_L > 1$, irreversible if $R_L = 0$ and linear if $R_L = 1$.⁶⁹⁻⁷¹

$$R_L = \frac{1}{1 + bC_i} \quad (4)$$

C_i is the initial Cu^{2+} concentration (mg dm^{-3}) and b is the Langmuir constant obtained from Table 4 ($\text{dm}^3 \text{mg}^{-1}$). All R_L values obtained in this study were found to fall between $0 < R_L < 1$, hence adsorption of Cu^{2+} onto MWCNT-COOH and MWCNT-ttpy is favourable.

The Langmuir isotherm assumes monolayer coverage of adsorbates onto the surface of adsorbent, while the Freundlich isotherm assumes that the surface of adsorbents is heterogeneous in nature.⁴ Since MWCNT-ttpy fit the Langmuir isotherm, it can be inferred that the active sites on this adsorbent are equivalent with a uniform surface, hence, the adsorbed Cu^{2+}

ions on this adsorbent do not interact with each other, achieving monolayer coverage of the adsorbate. In the case of MWCNT-COOH, the values of the Freundlich constant n indicate a favourable adsorption process since values were ≤ 10 (see Table 4).⁵⁴

Table 5 shows the results of some previously published studies investigating the sorption process of Cu^{2+} from aqueous solutions onto carbon-structured materials. These results were compared with those obtained in this study. A significant increase in sorption uptake of Cu^{2+} was obtained by using MWCNT-ttpy in comparison with 8-hydroxyquinoline-functionalized MWCNTs (8-HQ-MWCNT), also functionalized with a N-donor ligand but of lower denticity. Table 5 further demonstrates better uptake of Cu^{2+} on MWCNT-ttpy in comparison with composite adsorbents such as MWCNT/bagasse and MWCNT/ Fe_2O_4 . Thus, the results reported in this study compare very favourably with data obtained from other studies.

3.4.8. Thermodynamic parameters of adsorption. Thermodynamic parameters such as change in enthalpy (ΔH°), change in entropy (ΔS°) and change in Gibbs energy (ΔG°), were studied in order to examine the spontaneity of the adsorption process at varying temperatures. An adsorption process is considered feasible and spontaneous if negative values for ΔG° are obtained. The process is endothermic if the adsorption capacity (q_{eq}) increased with an increase in temperature and the reverse yields an exothermic process.

Table 4 Isotherm parameters for the adsorption of Cu^{2+} onto MWCNT-COOH and MWCNT-ttpy

Isotherm	Parameter	MWCNT-COOH				MWCNT-ttpy		
		293 K	303 K	313 K	318 K	303 K	313 K	318 K
Langmuir	$q_m/\text{mg g}^{-1}$	19.44	16.87	16.35	15.59	33.04	34.13	33.97
	$b/\text{dm}^3 \text{mg}^{-1}$	0.169	0.184	0.123	0.068	5.494	9.065	17.25
	RSE ^a	1.887	1.386	0.510	0.478	3.302	3.176	5.670
	SSR ^b	28.48	15.37	2.077	1.828	87.25	80.71	257.2
Freundlich	K_F	5.244	4.756	3.876	2.533	23.88	26.05	28.54
	n	3.056	3.188	2.964	2.507	6.641	7.006	8.991
	RSE	0.604	0.575	0.701	0.585	4.295	4.589	5.951
	SSR	2.922	2.644	3.926	2.740	147.6	168.5	283.3

^a RSE – residual square error. ^b SSR – sum of squared residuals.

Table 5 Comparison of Langmuir maximum capacity (q_m) for Cu^{2+} adsorbed onto various carbon-structured materials

Adsorbents	Conditions	$q_m/\text{mg g}^{-1}$	References
P-MWCNTs	pH 7.0, C_i 1.0 mg dm^{-3} , 250 mg dose, 120 min, 298 K	0.080	72
P-MWCNTs	pH 7.0, C_i 0.5 mg dm^{-3} , 125 mg dose, 120 min, 298 K	0.398	22
MWCNT-COOH	pH 7.0, C_i 20 mg dm^{-3} , 30 mg dose, 120 min, 293 K	12.34	10
8-HQ-MWCNT	pH 7.0, C_i 1.0 mg dm^{-3} , 250 mg dose, 120 min, 298 K	0.080	72
MWCNT/bagasse	pH 5.5, 100 mg dm^{-3} , 50 mg dose, 360 min, 301 K	15.60	24
MWCNT/ Fe_2O_4	pH 5.50, 10 mg dm^{-3} , 40 h, 353 K	8.920	25
MWCNT-COOH	pH 5.0, C_i 100 mg dm^{-3} , 50 mg dose, 24 h, 293 K	19.44	This study
MWCNT-ttpty	pH 5.0, C_i 100 mg dm^{-3} , 50 mg dose, 24 h, 293 K	31.65	This study

The change in Gibbs energy of adsorption (ΔG°) is calculated thus (eqn (5)):¹⁴

$$\Delta G^\circ = -RT \ln K \quad (5)$$

where ΔG° is the standard Gibbs energy change (J mol^{-1}), R is the universal gas constant ($8.314 \text{ J K}^{-1} \text{ mol}^{-1}$), and T is the absolute temperature in Kelvin. The value of K was obtained from the product of q_m and b obtained from the Langmuir plot (Table 4).^{69,73} The value of K was corrected to be dimensionless by multiplying by 1000.⁷⁴

A plot of $\ln K$ against $1/T$ was found to be linear, and the values of ΔH° and ΔS° were obtained from the slope and intercept of the plot, respectively, according to the van't Hoff equation (eqn (6)):

$$\ln K = -\frac{\Delta H^\circ}{RT} + \frac{\Delta S^\circ}{R} \quad (6)$$

Table 6 presents the thermodynamic parameters for the adsorption of Cu^{2+} onto MWCNT-COOH and MWCNT-ttpty. Negative values were obtained for ΔG° , indicating that the process was spontaneous and feasible for both adsorbents. An increase in negative values for ΔG° was obtained as the temperature of the adsorbate solution was increased for MWCNT-ttpty. This confirms that increasing the temperature of the adsorbate solution resulted in better sorption for the adsorbent. In contrast, a decrease in the negative values of ΔG° was obtained as temperature is increased when MWCNT-COOH was used as adsorbent. An exothermic process of adsorption was obtained with MWCNT-COOH, indicated by the negative ΔH° value obtained. On the other hand, the application of MWCNT-ttpty as adsorbent yielded an endothermic process, which is confirmed by the positive ΔH° value obtained.

Table 6 further shows a positive ΔS° value for MWCNT-ttpty, which indicates an increase in the disorderliness at the solid/solution interface resulting in a favourable adsorption process. However, a negative ΔS° was obtained for MWCNT-COOH indicating a decrease in disorderliness as the adsorbent interacts with the adsorbate. Hence, the adsorption process for MWCNT-ttpty is entropy-driven, while the process is enthalpy-driven for MWCNT-COOH. The values of ΔH° obtained show that the heat evolved/absorbed was greater than for physisorption ($2.1\text{--}20.9 \text{ kJ mol}^{-1}$), but lower than for chemisorption processes ($80\text{--}200 \text{ kJ mol}^{-1}$).^{4,75} This indicates that the

process for the removal of Cu^{2+} from aqueous solutions by using MWCNT-COOH and MWCNT-ttpty was a physico-chemical process,⁷⁵ indicating that adsorption was facilitated by both processes.

Thermodynamic parameters therefore suggest that the application of MWCNT-ttpty will be effective for remediating metal-polluted effluents discharged directly from industries.

3.4.9. Selectivity of MWCNT-ttpty towards the removal of different metal ions. The selectivity of the novel adsorbent was investigated to understand its sorption affinity for different metal ions in complex situations. A typical wastewater contains a mixture of metal ions, hence, the selectivity of an adsorbent towards metal ion removal is important. Adsorbate solutions containing equal initial metal ion concentrations between 10 and 50 mg dm^{-3} of Pb^{2+} , Cd^{2+} , Cu^{2+} and Zn^{2+} were conditioned to pH 5.5, and agitated in a thermostated water bath for 24 h, after the addition of 200 mg of MWCNT-ttpty. Fig. 11 shows a gradual decrease in the extent of removal as the initial concentration of metal ions was increased from 10 to 50 mg dm^{-3} . This was attributed to the competition for active sites amongst adsorbates as the initial metal ion concentration increased. At each metal ion concentration, the removal of Pb^{2+} from solution was highest, and Zn^{2+} exhibited the lowest efficiency (Fig. 11). It is worthy of note that the removal of Cu^{2+} from mixed metal ion solutions was considerably close to Pb^{2+} removal, obtaining efficiencies greater than 70% over the concentration range studied. This result signifies that MWCNT-ttpty was selective for Cu^{2+} , regardless of the presence of other metal ions in solution.

As proposed by Chen *et al.*,⁷⁶ the removal of divalent metal ions is inversely proportional to the hydrated radii of the metal

Table 6 Thermodynamic parameters for the adsorption of Cu^{2+} onto MWCNT-COOH and MWCNT-ttpty

Adsorbent	T/K	$\Delta G^\circ/\text{kJ mol}^{-1}$	$\Delta H^\circ/\text{kJ mol}^{-1}$	$\Delta S^\circ/\text{J K}^{-1} \text{ mol}^{-1}$
MWCNT-COOH	293	-19.72		
	303	-20.26		
	313	-19.79	-32.36	-99.19
	318	-18.42		
MWCNT-ttpty	293	-28.11		
	303	-30.50		
	313	-32.90	50.97	211.9
	318	-35.11		

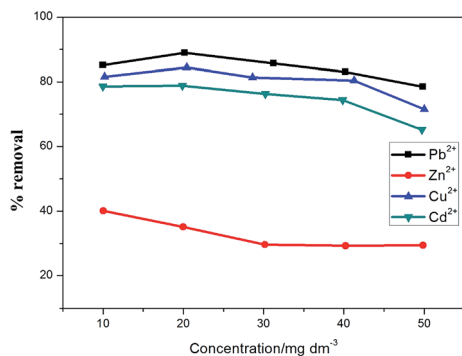


Fig. 11 The effect of equal initial metal ion concentration in a multi-component system for the adsorption of Pb²⁺, Zn²⁺, Cd²⁺ and Cu²⁺ [conditions: 25 cm³ of adsorbate solution, pH 5.5, 24 h equilibration time, adsorbent dose 200 mg, agitation speed 150 rpm, temperature 20 °C].

species in solution. The ionic radius of Pb²⁺, Cu²⁺, Cd²⁺ and Zn²⁺ are 1.33 Å, 0.71 Å, 0.95 Å and 0.83 Å respectively. The smaller the ionic radii of the metal ion species, the greater its tendency to hydrolyse, resulting in decreased sorption.^{24,76,77} Hence, the hydrated radii of the studied metal ions are in the order of Pb²⁺ (4.01 Å) < Cu²⁺ (4.19 Å) < Cd²⁺ (4.29 Å) < Zn²⁺ (4.30 Å).^{24,76,77} Metal ions with smaller hydrated radii therefore have easy access to the adsorbent sites, hence accounting for increased sorption in the sequence Pb > Cu > Cd > Zn (Fig. 11). Therefore, this principle could be said to be obeyed, since their removal was in the same order.

The selectivity of metal ions obtained in this study was mostly in agreement with previously reported studies. Srivastava *et al.*⁷⁸ and Li *et al.*⁷⁹ reported the same sequence order of Pb > Cu > Cd from a multicomponent system onto MWCNT-COOH. Sitko *et al.*⁸⁰ and Chen *et al.*⁷⁶ also reported similar trends in their studies by using graphene oxide and nano-hydroxyapatite, respectively. However, a sequence order of Pb > Cu > Zn > Cd was reported by Srivastava *et al.*⁸¹ and Sdiri *et al.*⁸² from a multicomponent system onto kaolinite and clay, respectively. This order was slightly different from that obtained in this study, hence, the removal of metal ion species is principally dependent on the textural characteristics of the sorbent used.

3.5. Analysis of real samples

In order to affirm the selectivity of MWCNT-ttpty and test its efficacy for metal ion removal in a real life scenario, water samples were collected from three different rivers in Durban, South Africa. The initial metal ion concentrations found in the water samples is given in Table S4.† Interestingly, a removal efficiency greater than 95% was obtained for all three metal ions in the three water samples (Table S4†). Although the initial concentrations of Pb²⁺, Cu²⁺ and Zn²⁺ in samples were in measurable amounts (≥10 mg dm⁻³), MWCNT-ttpty successfully sequestered these toxic heavy metal ions from the environmental samples. This further authenticates that MWCNT-ttpty and the method of adsorption presented are effective and

Table 7 Textural properties of spent-adsorbents after adsorption

Adsorbents	Surface area/m ² g ⁻¹	Pore volume/cm ³ g ⁻¹	Pore diameter/nm
MWCNT-COOH	104.22	0.314	15.18
MWCNT-ttpty	149.1	0.527	16.85

efficient when applied to real samples. Hence, the application of MWCNT-ttpty should be further explored for the remediation of wastewater or effluents discharged from industries.

3.6. Desorption studies

The process of desorption regenerates an adsorbent for reuse, thereby reducing the cost and availability of sorbents for adsorption. This process also limits the introduction of spent adsorbents into the environment, thereby reducing the disposal of secondary pollutants. Similarly, the isolation of copper is possible, and may encourage its reutilization for other valuable purposes.

Prior to the desorption of Cu²⁺ from loaded adsorbents, they were characterized by means of TEM and BET surface area measurements. These were performed in order to confirm the presence of adsorbate on the adsorbents. The data obtained exhibited lower surface areas and pore volumes for both adsorbents after adsorption as compared with their corresponding values before adsorption (Tables 7 vs. 1). This trend can be explained by the increase in agglomeration of nanotubes observed after adsorption as shown in Fig. S8.† The increase in CNT agglomeration after the deposition of Cu²⁺ onto their surface (Fig. S8†), resulted in a decrease in the surface areas exhibited by both adsorbents (Table 7). Further, the hydrated radius of Cu²⁺ (0.419 nm)^{24,77} is low compared with the pore volumes of the synthesized adsorbents (Table 1). Hence, copper species might fill the pore volumes of the adsorbent, thereby resulting in a reduction of the pore volumes of the adsorbents after adsorption (Table 7).

Desorption experiments were carried out by agitating a Cu²⁺-loaded adsorbent with 10 cm³ of 0.1 mol dm⁻³ HCl in a thermostated water bath at 20 °C for 30 min. The mixture was filtered and the final concentration of Cu²⁺ determined. Results obtained showed good desorption efficiencies of 62% and 73% for MWCNT-COOH and MWCNT-ttpty, respectively. These values signify that the adsorbents can be regenerated for reuse and the adsorbate solution can be isolated as chloride salt and reused for other industrial applications such as electroplating. Again, in this respect MWCNT-ttpty performed better, showing better desorption of Cu²⁺ than MWCNT-COOH.

4. Conclusions

A novel nanomaterial, synthesized by the use of 4'-(4-hydroxyphenyl)-2,2':6',2''-terpyridine as a modifier for acid-functionalized multiwalled carbon nanotubes (MWCNT-COOH), to produce nitrogen-functionalized MWCNTs (MWCNT-ttpty), was successfully synthesized. The adsorbent

proved effective and efficient for the removal of Cu^{2+} from aqueous solutions, obtaining a higher Langmuir monolayer adsorption capacity (q_m) of 31.65 mg g^{-1} than the 19.44 mg g^{-1} obtained for MWCNT-COOH. Also, a higher sorption uptake of Cu^{2+} was exhibited by MWCNT-ttpty when compared with other MWCNT-containing sorbents from other studies.

This study revealed that MWCNT-ttpty can be used as an alternative adsorbent for the removal of heavy metal ions from municipal wastewater and industrial effluents, due to the high efficiency exhibited towards Cu^{2+} removal from aqueous solution. The regeneration of this adsorbent was successful, suggesting that the spent adsorbent and Cu^{2+} can be recovered and made available for reuse, and thereby reducing secondary pollutants.

Acknowledgements

The authors wish to thank the University of KwaZulu-Natal, Durban, for research facilities and the National Research Foundation (NRF) for provision of funds for the completion of this work.

References

- Z. Zhao, Z. Yang, Y. Huc, J. Li and X. Fan, *Appl. Surf. Sci.*, 2013, **276**, 476–481.
- N. Arora and N. N. Sharma, *Diamond Relat. Mater.*, 2014, **50**, 135–150.
- L. M. Ombaka, P. Ndungu and V. O. Nyamori, *Catal. Today*, 2013, **217**, 65–75.
- O. A. Oyetade, V. O. Nyamori, B. S. Martincigh and S. B. Jonnalagadda, *RSC Adv.*, 2015, **5**, 22724–22739.
- B. Pan and B. Xing, *Environ. Sci. Technol.*, 2008, **42**, 9005–9013.
- G. Keru, P. G. Ndungu and V. O. Nyamori, *Int. J. Energy Res.*, 2014, **38**, 1635–1653.
- L. M. Ombaka, P. G. Ndungu and V. O. Nyamori, *RSC Adv.*, 2014, **5**, 109–122.
- L. Hou and D. Li, *Inorg. Chem. Commun.*, 2005, **8**, 190–193.
- M. Chua and C.-K. Chui, *J. Mech. Behav. Biomed. Mater.*, 2015, **44**, 164–172.
- I. Mobasherpour, E. Salahi and M. Ebrahimi, *J. Saudi Chem. Soc.*, 2014, **18**, 792–801.
- C. M. A. Iwegbue, *Vet. Arh.*, 2008, **78**, 401–410.
- I. Giannopoulou and D. Panias, *Hydrometallurgy*, 2008, **90**, 137–146.
- M. Abdel Salam, G. Al-Zhrani and S. A. Kosa, *J. Ind. Eng. Chem.*, 2014, **20**, 572–580.
- Y.-S. Ho, *Water Res.*, 2003, **37**, 2323–2330.
- P. L. Homagai, K. N. Ghimire and K. Inoue, *Bioresour. Technol.*, 2010, **101**, 2067–2069.
- H. D. Özsoy, H. Kumbur and Z. Özer, *Int. J. Environ. Pollut.*, 2007, **31**, 125–134.
- M. G. A. Vieira, A. F. de Almeida Neto, M. G. C. Da Silva, C. N. Carneiro and A. A. Melo Filho, *Braz. J. Chem. Eng.*, 2014, **31**, 519–529.
- S. Sai Bhargav and I. Prabha, *Int. J. Chem. Biol. Eng.*, 2013, **3**, 107–112.
- Y. S. Ho and G. McKay, *Water, Air, Soil Pollut.*, 2004, **158**, 77–97.
- H. Liu, S. Feng, N. Zhang, S. Du and Y. Liu, *Front. Environ. Sci. Eng.*, 2014, **8**, 329–336.
- Y. Jiang, H. Pang and B. Liao, *J. Hazard. Mater.*, 2009, **164**, 1–9.
- M. Abdel Salam, *Int. J. Environ. Sci. Technol.*, 2013, **10**, 677–688.
- M. S. Tehrani, P. A. Azar, P. Ehsani Namin and S. M. Dehaghi, *J. Appl. Environ. Biol. Sci.*, 2014, **4**, 316–326.
- I. A. A. Hamza, PhD Thesis, University of KwaZulu-Natal, Durban, South Africa, 2013.
- J. Hu, D. Zhao and X. Wang, *Water Sci. Technol.*, 2011, **63**, 917–923.
- S. R. Popuri, R. Frederick, C.-Y. Chang, S.-S. Fang, C.-C. Wang and L.-C. Lee, *Desalin. Water Treat.*, 2013, **52**, 691–701.
- S. Biniak, G. Szymanski, J. Siedlewski and A. Swiatkowski, *Carbon*, 1997, **35**, 1799–1810.
- H. P. Boehm, *Carbon*, 2002, **40**, 145–149.
- T. A. Khan, M. Nazir and E. A. Khan, *Toxicol. Environ. Chem.*, 2013, **95**, 919–931.
- M. N. Patel, P. A. Dosi and B. S. Bhatt, *Med. Chem. Res.*, 2012, **21**, 2723–2733.
- M. N. Patel, H. N. Joshi and C. R. I. Patel, *Polyhedron*, 2012, **40**, 159–167.
- S. Santangelo, G. Messina, G. Faggio, S. H. Abdul Rahim and C. Milone, *J. Raman Spectrosc.*, 2012, **43**, 1432–1442.
- J. Shen, W. Huang, L. Wu, Y. Hu and M. Ye, *Mater. Sci. Eng., A*, 2007, **464**, 151–156.
- N. Sakai, T. Moriya and T. Konakahara, *J. Org. Chem.*, 2007, **72**, 5920–5922.
- Y. S. Ho, *Water Res.*, 2004, **38**, 2962–2964.
- Y.-S. Ho, *J. Hazard. Mater.*, 2006, **136**, 681–689.
- S. H. Chien and W. R. Clayton, *Soil Sci. Soc. Am. J.*, 1980, **44**, 265–268.
- E. Demirbas, M. Kobya, E. Senturk and T. Ozkan, *Water SA*, 2004, **30**, 533–539.
- I. Langmuir, *J. Am. Chem. Soc.*, 1918, **40**, 1361–1402.
- H. Freundlich, *Z. Phys. Chem.*, 1906, **57**, 385–470.
- M. I. Temkin and V. Pyzhev, *Acta Phys. Chim.*, 1940, **12**, 327–356.
- M. M. Dubinin and L. V. Radushkevich, *Proc. Acad. Sci. USSR, Phys. Chem. Sect.*, 1947, **55**, 327–329.
- R. Sips, *J. Chem. Phys.*, 1948, **16**, 490–495.
- J. Toth, *Acta Chim. Acad. Sci. Hung.*, 1971, **69**, 311–328.
- O. Redlich and D. L. Peterson, *J. Phys. Chem.*, 1959, **63**, 1024.
- A. R. Khan, I. R. Al-Waheab and A. Al-Haddad, *Environ. Technol.*, 1996, **17**, 13–23.
- The R Development Core Team, *The R foundation for statistical Computing, R version 3.0.2*, 2013.
- S. Narimany and S. Ghammamy, *Global J. Pharmacol.*, 2013, **7**, 187–191.
- T. L. Yang, W. W. Qin, Z. F. Xiao and W. S. Liu, *Chem. Pap.*, 2005, **59**, 17–20.

- 50 W. Huang, C. Li, J. Wang and L. Zhu, *Spectrosc. Lett.*, 1998, **31**, 1793–1809.
- 51 I. D. Rosca, F. Watari, M. Uo and T. Akasaka, *Carbon*, 2005, **43**, 3124–3131.
- 52 K. Chizari, A. Vena, L. Laurentius and U. Sundararaj, *Carbon*, 2014, **68**, 369–379.
- 53 Z. Wang, M. D. Shirley, S. T. Meikle, R. L. D. Whitby and S. V. Mikhailovsky, *Carbon*, 2009, **47**, 73–79.
- 54 K. S. Tong, M. J. Kassim and A. Azraa, *Chem. Eng. J.*, 2011, **170**, 145–153.
- 55 M. A. Salleh, D. K. Mahmoud, W. A. Abdul Karim and A. Idris, *Desalination*, 2011, **280**, 1–13.
- 56 R. M. Smith and A. E. Martell, *Critical Stability Constants*, Plenum Press, New York, 1976, p. 6.
- 57 P. Gans, *HySS, version 4.0.31*, 2009.
- 58 K. V. Kumar, *J. Hazard. Mater.*, 2006, **137**, 1538–1544.
- 59 J. Lin and L. Wang, *Front. Environ. Sci. Eng.*, 2009, **3**, 320–324.
- 60 Y. S. Ho and C. C. Wang, *Process Biochem.*, 2004, **39**, 759–763.
- 61 Y. S. Ho and G. McKay, *Process Biochem.*, 1999, **34**, 451–465.
- 62 B. Yu, Y. Zhang, A. Shukla, S. S. Shukla and K. L. Dorris, *J. Hazard. Mater.*, 2000, **B80**, 33–42.
- 63 S. G. Muntean, M. E. Radulescu-Grad and P. Sfarloaga, *RSC Adv.*, 2014, **4**, 27354–27362.
- 64 C. H. Wu, *J. Hazard. Mater.*, 2007, **144**, 93–100.
- 65 Y. Yao, F. Xu, M. Chen, Z. Xu and Z. Zhu, *Bioresour. Technol.*, 2010, **101**, 3040–3046.
- 66 F. Ekmekyapar, A. Aslan, Y. K. Bayhan and A. Cakici, *J. Hazard. Mater.*, 2006, **137**, 293–298.
- 67 T. A. Khan, S. Dahiya and I. Ali, *Appl. Clay Sci.*, 2012, **69**, 58–66.
- 68 Y.-S. Ho, *Scientometrics*, 2004, **59**, 171–177.
- 69 I. A. A. Hamza, B. S. Martincigh, J. C. Ngila and V. O. Nyamori, *Phys. Chem. Earth*, 2013, **66**, 157–166.
- 70 O. Soon-An, S. Chye-Eng and L. Poh-Eng, *EJEAFChe, Electron. J. Environ., Agric. Food Chem.*, 2007, **6**, 764–1774.
- 71 T. K. Sen and D. Gomez, *Desalination*, 2011, **267**, 286–294.
- 72 S. A. Kosa, G. Al-Zhrani and M. Abdel Salam, *Chem. Eng. J.*, 2012, **181–182**, 159–168.
- 73 R. Djeribi and Q. Hamdaoui, *Desalination*, 2008, **225**, 95–112.
- 74 S. K. Milonjić, *J. Serb. Chem. Soc.*, 2007, **72**, 1363–1367.
- 75 Y. Liu and Y.-J. Liu, *Sep. Purif. Technol.*, 2008, **61**, 229–242.
- 76 S. B. Chen, Y. B. Ma, L. Chen and K. Xian, *Geochem. J.*, 2010, **44**, 233–239.
- 77 L. Lv, G. Tsoi and X. Zhao, *Ind. Eng. Chem. Res.*, 2004, **43**, 7900–7906.
- 78 S. Srivastava, *Adv. Mater. Lett.*, 2013, **4**, 2–8.
- 79 Y.-H. Li, J. Ding, Z. Luan, Z. Di, Y. Zhu, C. Xu, D. Wu and B. Wei, *Carbon*, 2003, **41**, 2787–2792.
- 80 R. Sitko, E. Turek, B. Zawisza, E. Malicka, E. Talik, J. Heimann, A. Gagor, B. Feist and R. Wrzalik, *Dalton Trans.*, 2013, **42**, 5682–5689.
- 81 P. Srivastava, B. Singh and M. Angove, *J. Colloid Interface Sci.*, 2005, **290**, 28–38.
- 82 A. Sdiri, T. Higashi, R. Chaabouni and F. Jamoussi, *Water, Air, Soil Pollut.*, 2011, **223**, 1191–1204.